An Atomic-Level Perspective on the interactions between Organic Pollutants and PET particles: A Comprehensive Computational and DFT Investigation

Anamarija Pulitika, Panagiotis Karamanis, Marin Kovačić, Ana Lončarić Božić, Hrvoje Kušić

ChemPhysChem

Chemistry Europe
European Chemical Societies Publishing

Accepted Article

Title: An Atomic-Level Perspective on the interactions between Organic Pollutants and PET particles: A Comprehensive Computational and DFT Investigation

Authors: Anamarija Pulitika, PANAGIOTIS Karamanis, Marin Kovačić, Ana Lončarić Božić, and Hrvoje Kušić

To be cited as: *ChemPhysChem* **2024**, e202300854

Link to VoR: https://doi.org/10.1002/cphc.202300854

WILEY VCH

10.1002/cphc.202300854

An Atomic-Level Perspective on the interactions between Organic Pollutants and PET particles: A Comprehensive Computational Investigation

Anamarija Pulitika[a], Panaghiotis Karamanis[b]*, Marin Kovačić[a], Ana Lončarić Božić[a], Hrvoje Kušić[a]

[a] University of Zagreb Faculty of Chemical Engineering and Technology, 10000 Zagreb, Croatia

[b] E2S UPPA, CNRS, IPREM, Université de Pau et des Pays de l'Adour, 64053 Pau, France

*Corresponding author: P. Karamanis: panagiotis.karamanis@univ-pau.fr

10.1002/cphc.202300854

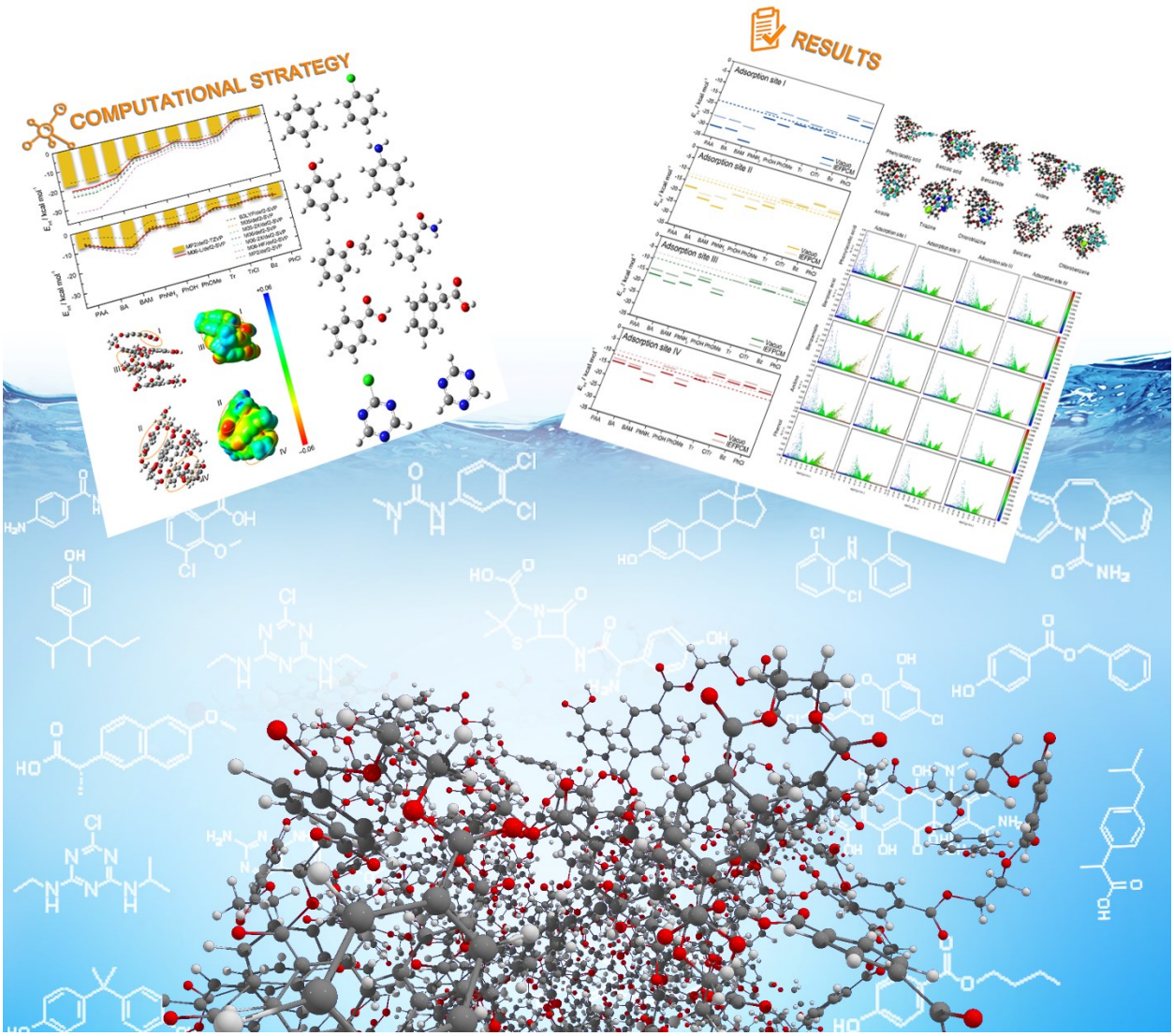

10.1002/cphc.202300854

Abstract

Microplastics (MPs) have recently attracted a lot of attention worldwide due to their abundance and potentially harmful effects on the environment and on human health. One of the factors of concern is their ability to adsorb and disperse other harmful organic pollutants in the environment. To properly assess the adsorption capacity of MP for organic pollutants in different environments, it is pivotal to understand the mechanisms of their interactions in detail at the atomic level. In this work, we studied interactions between polyethylene terephthalate (PET) MP and small organic pollutants containing different functional groups within the framework of density functional theory (DFT). Our computational outcomes show that organic pollutants mainly bind to the surface of a PET model via weak non-bonding interactions, mostly hydrogen bonds. The binding strength between pollutant molecules and PET particles strongly depends on the adsorption site while we have found that the particle size is of lesser importance. Specifically, carboxylic sites are able to form strong hydrogen bonds with pollutants containing hydrogen bond donor or acceptor groups. On the other hand, it is found that in such kind of systems π-π interactions play a minor role in adsorption on PET particles.

Keywords: microplastics, nanoplastics, polyethylene terephthalate, adsorption, DFT

Introduction

Growing plastic production and the accumulation of plastic waste in the environment have been well-known global problems for a long time. But recently, the focus was turned to microplastics (MPs), plastic particles smaller than 5 millimetres in diameter that are formed by fragmentation of larger plastics. Due to their small size and light weight, MPs can be easily transported and are now found in every environmental compartment around the world, including freshwater, seas, oceans, soils, indoor and outdoor air, and even polar ice.[1,2] MPs are highly persistent, and because of their abundance, the number of their potential sources, and the potential risk they could pose, they are considered contaminants of emerging concern.[3] Most research involving MP addresses freshwater and marine MPs. MPs in water can easily be ingested by small organisms and thus enter the food chain, potentially causing toxic effects in organisms. The accumulation of MPs in freshwater zebrafish *Danio rerio* showed toxic effects leading to intestinal and liver damage, reproductive system dysfunction, oxidative stress, and induced mortality.[4,5] In addition, MPs can adsorb other environmental pollutants on their surface. The adsorption and desorption of pollutants on the surface of MPs may increase the overall toxicity.[6,7] Therefore, to properly evaluate the potential risk of MPs, it is important to understand the mechanism of interaction between MPs and other pollutants in the environment.

Due to its large specific surface area and hydrophobicity, MPs have shown the ability to accumulate organic pollutants on its surface and transport them in the environment.[8] Adsorption of organic pollutants to MPs is a very complex process that depends on the physicochemical properties of both MPs and organic pollutants, as well as environmental factors. As a result, several experimental attempts to study the adsorption of organic pollutants on MPs have led to divergent results. For instance, in three different studies, the adsorption constants (K_d) of sulfamethoxazole adsorption on PE MP were 700 $dm^3\ kg^{-1}$,[9] 592 $dm^3\ kg^{-1}$,[10] and 30 $dm^3\ kg^{-1}$.[11] High variation in results and experimental designs make it difficult to draw definite conclusions.

The so far reported experimental studies suggest/claim that the adsorption capacity of MPs is generally higher for hydrophobic pollutants.[9,12] At the atomic level, it is believed that the ability of pollutants and MP to interact by π–π interactions, hydrogen bonds, and electrostatic interactions can affect the adsorption capacity. Li et al.[13] showed that the adsorption of ciprofloxacin and amoxicillin on polyaniline (PA) MPs is an order of magnitude higher than on polyethylene (PE),

polystyrene (PS), polypropylene (PP) and polyvinyl chloride (PVC). They attributed theses effects to the ability of PA to form hydrogen bonds, without though providing complete evidence. In another work, Munoz et al.[14] reported that the adsorption of diclofenac on PS and polyethylene terephthalate (PET) is higher than on PP and PE. Their PS has a higher adsorption capacity for aromatic pollutants such as diethyl-phthalate and dibutyl-phthalate than PE and PVC possibly due to additional π–π interactions that may further increase their adsorption capacity.[15] Based on their experimental results Yang et al.[12,16] proposed that π-π interactions should not play an important role on the adsorption on PET MPs. In same context, Liu et al.[12] proposed that the weaken π–π interactions between PET and aromatic pollutants is due to the presence of the electron-withdrawing ester "fragments" of the backbone of PET chains.

Although many studies have addressed the adsorption capacity of MP for various organic pollutants, the interaction mechanism is still not well understood. Density functional theory methods (DFT) can be used to calculate adsorption energies to further elucidate the interactions between MPs and organic pollutants. Mo et al.[17] calculated the adsorption of carbendazim and carbofuran on PE and PP chain and showed that adsorption is mainly controlled by weak van der Waals interactions. Yu et al.[18] calculated the interactions between naphthalene and four of its derivatives ($–NH_2$, $–CH_3$, –COOH, –OH) and a short five member PS chain. Their results pointed out that different functional groups incorporated on naphthalene may decrease their adsorption capacity.

The studies mentioned above used single oligomeric chains as MP models. However, Cortés-Arriagada argued that such an approach is expected to underestimate the contribution of dispersion forces and that a folded (nano)particle model should be used instead.[19,20] The adsorption of pollutants on MPs is controlled by several interactions, all of which contribute to the total adsorption energy.[21] It is suggested that the interactions with organic pollutants and model MP are consistent for realistic microplastics and nanoplastics.[22] However, the contribution of each interaction and the effects of the structure and functional groups of the pollutants remain unclear. A molecular dynamics study by Liu et al.[23] shows that even small PE and PS nanoparticles can load many aromatic hydrocarbons in water. Since the structure of MPs is not uniform, the adsorption interaction could be different at different parts of the MP surface. Additionally, the ageing of MPs in the environment can lead to chain breaking and the formation

10.1002/cphc.202300854

of new functional groups on the surface. Therefore, the interactions between mPET and other pollutants should be studied considering various adsorption sites.

In this work, we computationally investigate and compare the effects of different functional groups commonly found in water pollutants such as pesticides, pharmaceuticals, and personal care products on adsorption interactions. We chose a neutral model for the PET model as an opening step to isolate specific interaction mechanisms like hydrogen bonding and van der Waals forces. This choice serves as a baseline for future studies that may incorporate charged models to capture a broader range of interactions. PET microplastics (MPs) were selected for this study due to their widespread environmental presence and significant impact on both ecological systems and human health.[24,25] Adsorption interactions were examined at multiple sites on the PET nanoplastic surface to mimic the complexity of real-world. To ensure the robustness of our findings, we employed multiple DFT methods, serving as both a validation and a sensitivity test for our computational approach. This comparative analysis allows for a more reliable interpretation of interaction energies, thereby contributing to a deeper understanding of the role of PET MPs in contaminant transport and bioaccumulation.

Computational details

All calculations were performed with Gaussian 16 software for solving the electronic structure equations.[26] Geometry optimizations and interaction energy computations have been performed with the M06-L combined with the def2-SVP basis set. Vibrational frequencies were calculated to ensure that the studied systems are true minima of the corresponding potential energy surfaces. Grimme's 3D empirical dispersion and density fitting were used in all computations. M06-L is a non-hybrid density functional developed by the Truhlar group, and it is part of the Minnesota family of DFT functionals. It has been developed to treat non-covalent interactions, thermochemistry, and thermochemical kinetics more accurately. One of the notable strengths of M06-L is its robust performance across a diverse range of molecular systems and properties, apart of the fact that is considerably less computationally expensive than conventional hybrid functionals. A detailed assessment of its performance with respect to more computationally demanding methods is given in supporting materials and the results are shown in **Figure S1-S5** and **Table S1-S5**. Specifically, we tested the performance of M06-L with respect to second order Møller–Plesset (MP2) perturbation approximation and the widely applied hybrid functionals B3LYP,[27–30] which combines Hartree-Fock exchange with gradient-corrected correlation. Also we considered M05,[31] known for its accurate treatment of non-covalent interactions, M05-2X,[32] the range-separated hybrid exchange-correlation functional and M06[33] functional optimized for main-group thermochemistry, thermochemical kinetics, and non-covalent interactions. Finally we considered M06-2X,[33] a global hybrid with increased Hartree-Fock exchange and M06-HF.[34]

The construction of the polyethylene terephthalate (PET) model was initiated by optimizing a starting configuration consisting of two dimers of terephthalic acid. Following each optimization cycle, a monomeric unit was appended to each of the existing chains. The iterative optimization led to a final model built from 138 atoms ($C_{60}H_{52}O_{26}$), hereafter referred to as mPET. The Cartesian coordinates of the optimized final geometry are listed in **Table S6** of the supporting materials. mPET features two interacting chains, each composed of three monomeric units. This configuration was chosen as the representative model particle since additional extensions in the chain length were found to have negligible impact on the adsorption interactions under investigation.

The surface of mPET was analysed based on its molecular electrostatic surface potentials (MEP) to locate potential adsorption sites representing different parts of PET molecule. The

selected adsorption sites include part of the PET near the terminal carboxyl group, near the benzene ring of PET, and part of mPET surface that is not near the terminal groups of the polymer chains. MP showed the ability to accumulate a large concentration of pollutants. To understand the effects of adsorption at one site on adsorption at another adsorption site, the interactions of phenol with mPET were also calculated in the presence of other adsorbed phenols.

The interaction energies (E_{int}) were calculated as:

$$E_{\mathrm{int}} = E_{\mathrm{mPET/pollutant}} - E_{\mathrm{mPET}} - E_{\mathrm{pollutant}}$$

Where $E_{\mathrm{mPET/pollutant}}$ is the total energy of mPET−pollutant complex, E_{mPET} the energy of mPET unit, and $E_{\mathrm{pollutant}}$ the energy of a pollutant unit. The stronger the interaction, the more negative the E_{int} becomes. Using a rich basis set to calculate the energy of the complex compared to the energy of single units leads to the overestimation of interaction energies due to the basis set superposition error (BSSE). To rectify BSSE, the classical counterpoise correction (CP) method was used.[35,36] The CP method determines the energy of each unit of the complex using the basis set of a whole complex by representing the atoms of the other unit as "ghost atoms" characterized by the absence of nuclear charges and electrons. The geometry of the individual units remains the same as it was in the complex. IEFPCM model[37] was used to calculate interactions in the implicit water solvent.

Analysis of intermolecular weak interactions was performed in IGMPlot-3.08 program[38] using Independent gradient model based on Hirshfeld partition of molecular density (IGMH).[39,40] In IGMH method, the function of interfragmentary interaction region ($\delta g^{\mathrm{inter}}$) is defined as follows:

$$\delta g^{\mathrm{inter}}(\mathrm{r}) = g^{\mathrm{IGM,inter}}(\mathrm{r}) - g^{\mathrm{inter}}(\mathrm{r})$$

where $g^{\mathrm{IGM,\,inter}}$ is the sum of density gradient magnitude of all fragments and g^{inter} is the magnitude of superposition of density gradient of all fragments. To visualize weak interactions, the product of the electron density function (ρ) and the sign of the second largest eigenvalue of Hessian matrix of electron density ($sign(\lambda_2)$) is mapped on the isosurface of $\delta g^{\mathrm{inter}}$. $sign(\lambda_2)$ is the sign of the second largest eigenvalue of Hessian matrix of electron density. A negative $sign(\lambda_2)$ is attributed to attractive interactions, while a positive sign is attributed to non-bonding interactions. The electron density (ρ) indicates the strength of the interactions in such a way that the electron density is greater in regions where attractive or repulsive forces are stronger. Visual

10.1002/cphc.202300854

Molecular Dynamics (VMD) program[41] is used alongside IGMPlot to generate colour-filled isosurface and gnuplot 5.4 program[42] to generate colour mapped scatter plot.

10.1002/cphc.202300854

Modeling organic pollutants

In **Figure 1** we show the molecular structure of some common pharmaceuticals, pesticides and personal care products. This group of potential water pollutants includes those containing aromatic rings with different functional groups. The hydroxyl functional group is found in pollutants such as 17β-estradiol and amoxicillin, nonylphenol, benzylparaben and butylparaben, and bisphenol A. Common pollutants with carboxyl groups are diclofenac and ibuprofen. Naproxen and oxybenzone contain a methoxy group, among others. The amide functional group is a component of oxytetracycline and carbamazepine, the amine group of trimethoprim and procainamide. Chlorine is contained in diuron, triclosan and triclocarban. Dicamba is a pesticide containing a benzene ring with carboxyl and methoxy groups and two chlorines. In this group we also include atrazine and simazine, common pesticides that have triazine in their structure.

A careful examination of their molecular structures points out that all systems considered feature some mutual functional groups, which are expected to play an important role in their interaction with the surface of a given microplastic particle, especially those having in their pristine or aged forms oxygen containing groups, such as hydroxyls, carbonyls and carboxyls. These functional groups are represented by the simple molecules illustrated in **Figure 2**. For the sake of computational efficiency, while still capturing essential chemical interactions, we considered these reference molecular entities as model water pollutants.

10.1002/cphc.202300854

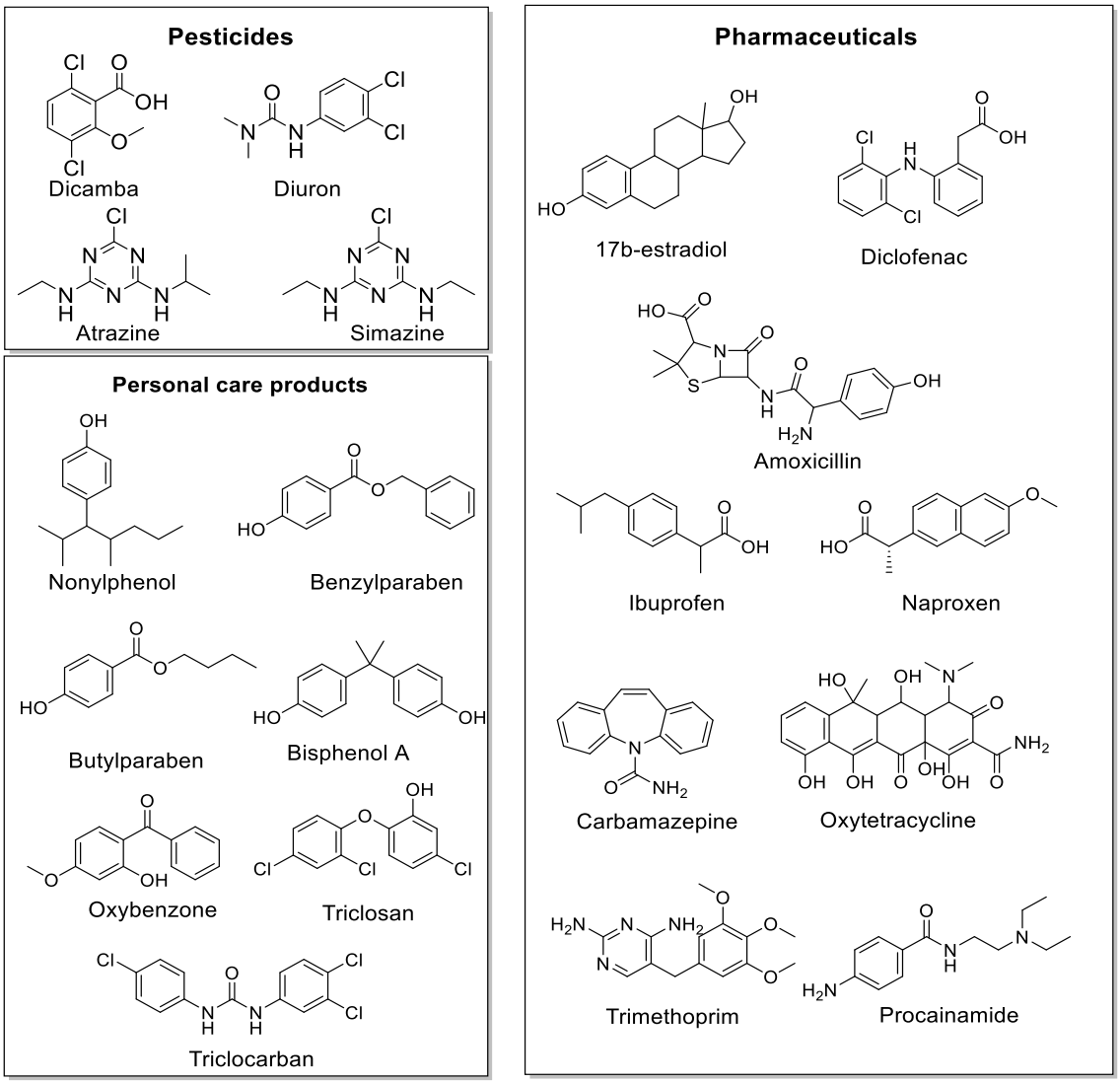

Figure 1. Structures of common organic pollutants in water.

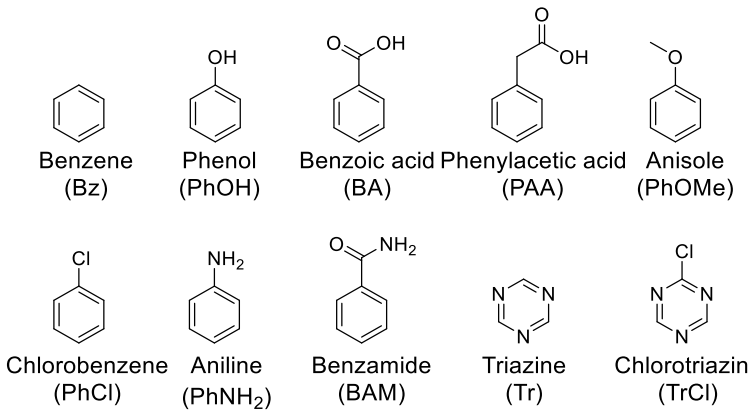

Figure 2. Organic pollutant molecular models.

10.1002/cphc.202300854

Results and discussion

PET models adsorption sites and size effects

Polyethylene terephthalate is composed by elongated polymer chains that are held together through noncovalent intermolecular forces. The predominant types of noncovalent interactions in PET are van der Waals forces, particularly dispersion forces, leading to induced dipole moments that cause attraction between neighboring chains. To obtain an estimation of the strength of these forces we computed first the interaction energies of two chains in PET as a function of "the number of ***PET*** units". The results depicted in **Figure 3** suggest that the interaction energies converge to a value of about –9 kcal mol^{-1} per unit at the M06-L level of theory.

In **Figure 4** we have plotted the electrostatic potential map (MEP**)** of a PET model built from 2 chains of 3 monomers. As seen, there are some distinct areas of excess negative and positive charges which are expected to act as adsorption sites of a given pollutant through electrostatic interactions. Specifically for the PET model considered, we found four potential sites of interest. The adsorption site I is the carboxyl group at the end of the PET chain. This adsorption site is not so common in real polymers given the limited number of terminal units relative to the overall surface area. However, the ageing of microplastic in nature may lead to chain breakage and the formation of new oxygen-containing functional groups, increasing the number of sites similar to adsorption site I, which could alter the adsorption capacity of pollutants. The adsorption site II is a benzene ring fused in a PET chain chosen to study the importance of π-π interactions. Finally, adsorption sites III and IV represent the surface of PET, far from terminal units. We assume that those four adsorption sites are the most common ones on the surface of micro-sized particles and could determine the adsorption.

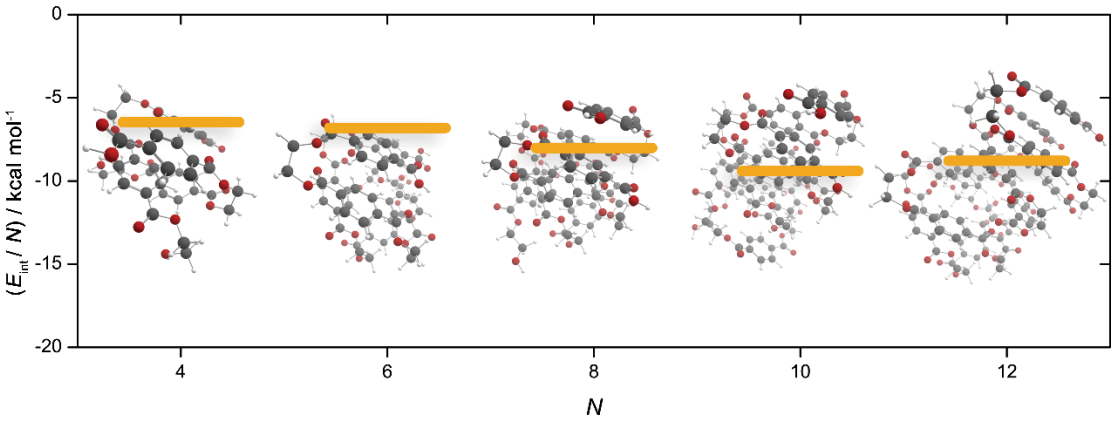

10.1002/cphc.202300854

Figure 3. Interaction energies per monomer of two PET chains optimized in gas phase at M06-L level of theory and def2-SVP basis set.

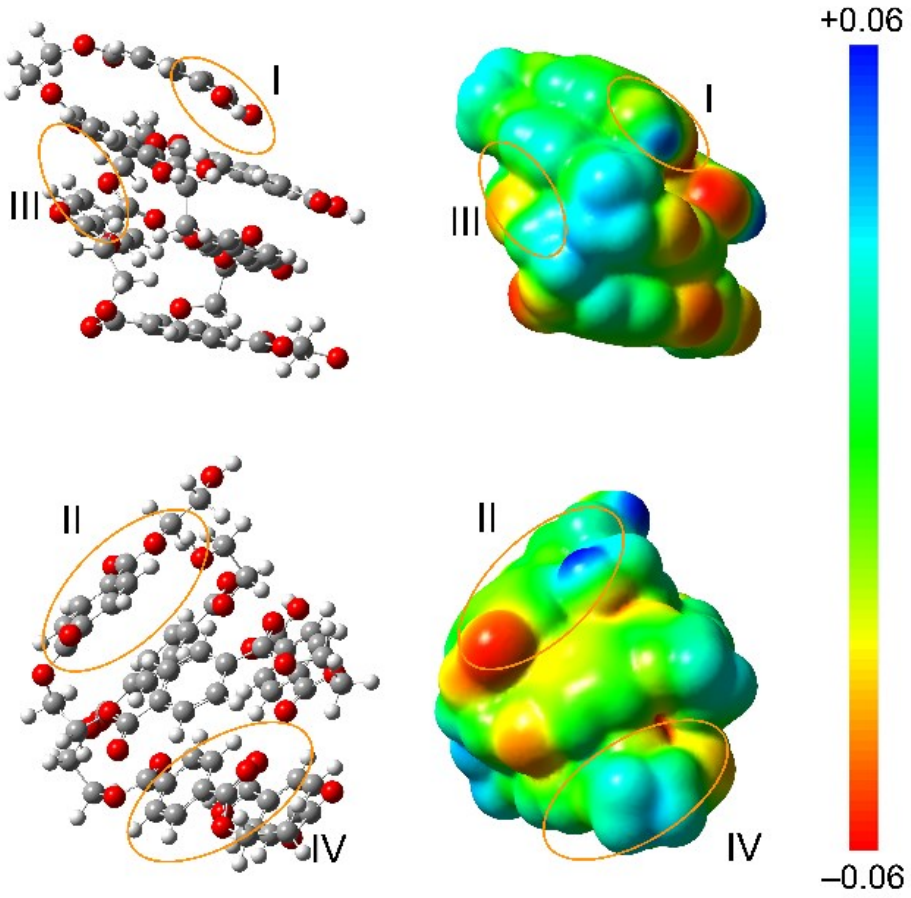

Figure 4. Structure and molecular electrostatic potential (MEP) of mPET. Red parts represent the excess of negative charge on the surface, and blue excess of positive charge. Adsorption sites I, II, III and IV are circled with orange lines.

To test the effect of PET model size on the interactions of pollutants, we compared the interaction energies of phenol, one of the representatives of our model pollutants, with the PET models of two different sizes. The first model consisting of two chains with three monomers has a total of 138 atoms and 620 electrons, and is about 1 nm long. The second model is twice as large, so it consists of 2 chains with 6 monomers and is about 2 nm long. The interaction energies between phenol and the two models were calculated for adsorption sites I and II. The results shown in **Figure 5** indicate that increasing the size of PET does not significantly affect the adsorption energy. Therefore, for the sake of computational efficiency, in this work we considered a model representing a PET microparticle composed of two chains of 3 units, hereafter referred to as mPET.

10.1002/cphc.202300854

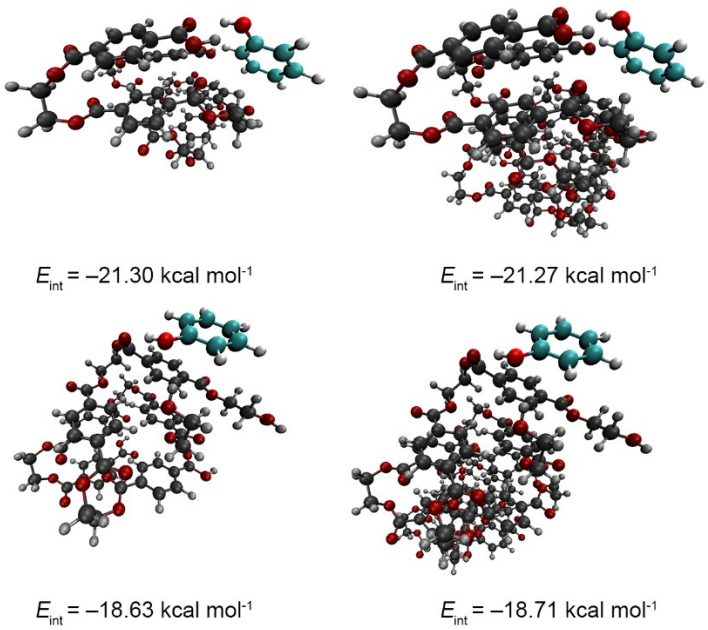

Figure 5. The effect of model PET size on the interaction energy of phenol and adsorption sites I and II of mPET calculated by M06-L/def2-SVP method.

Molecular Interactions.

In **Figure 6**. we show the results of the interaction energies of our model organic pollutants and mPET at the four adsorption sites we selected. We also compare these interaction energies with those of the water molecule for the obvious reasons. Upon a careful analysis of the data referring to the adsorption site I (**Figure 6a**) which refers to the terminal carboxyl group, it becomes evident that one could classify the considered model-pollutants into three groups based on their interaction energies with adsorption site I. The first group consists of phenylacetic acid, benzoic acid, and benzamide, which can form two strong hydrogen bonds with the terminal carboxyl group. Their interaction energy with adsorption site I is about –31 kcal mol^{-1}, which is much stronger than the interactions between adsorption site I and the water molecule. Therefore, it is reasonable to speculate that these model pollutants could, to a certain extent, adsorb onto PET in an aqueous environment. Aniline, phenol, anisole, triazine, and chlorotriazine can be placed in the second group because their interaction energies with adsorption site I are about –20 kcal mol^{-1}, which is comparable to the interaction energies of the water molecule and adsorption site I. Benzene and chlorobenzene are in the last group, since their interaction energies with adsorption site I are only about –11 kcal mol^{-1}, which is about two times weaker than the interaction of the

water molecule. Compared with the interaction energies calculated in vacuum, those calculated in PCM are found on average 5 kcal mol^{-1} weaker for the first group of model pollutants, 2 kcal mol^{-1} weaker for the second, and about 1.5 kcal mol^{-1} weaker for the third group, and the interaction energy of water did not change. Nevertheless, the observed trend remains the same. Energy decomposition analysis (EDA) using the sobEDA method introduced by Lu and Chen,[43] performed with terephthalic acid instead of mPET and some of the considered model pollutants (see Figure S6) suggests that the stability of these species on absorption site I arises from a balance between electrostatic/orbital attractive forces and exchange-repulsion. The specific trend varies from one model pollutant to another, leading to differences in the overall stability of their adsorption complexes. For instance, the obtained sobEDA data indicates that the type of functional groups in the adsorbate pollutants might have a significant impact on electrostatic interactions. Specifically, species with electron-withdrawing groups (like nitro, carbonyl, or cyano groups) might exhibit stronger electrostatic attractions due to increased polarity, whereas electron-donating groups (like methyl or methoxy) could result in weaker electrostatic attractions. Furthermore, it is confirmed that compounds able to form hydrogen bonds can bind stronger on mPET via hydrogen bonding interactions with the carboxyl groups on mPET.

The results for adsorption site II are shown in the **Figure 6b**. This site is a benzene ring with a hydroxyl terminal group in its vicinity. The average energy of phenylacetic acid, benzoic acid and benzamide is –20 kcal mol^{-1}, which is only 3 kcal mol^{-1} stronger than the average interaction energies of aniline, phenol, and anisole. In contrast, triazine and chlorotriazine exhibit even weaker interaction energies averaging around –12kcal/mol which is comparable to the interaction energy of the water molecule. For benzene and chlorobenzene, the average interaction energies with adsorption site II are around –10 kcal mol^{-1}.

Let us now turn our attention to adsorption sites III and IV which are located on two separate parts of the mPET surface "far" from the terminal groups. Hydrogen bonding at these sites can occur exclusively between the proton donor groups present in our model pollutants and the oxygen atoms of ester groups in the mPET structure. The interaction energies of the water molecule and the latter adsorption sites are found about –9 kcal mol^{-1} for III and –11 kcal mol^{-1} for IV as illustrated in **Figures 6c** and **6d**. A consistent trend is evident across both sites. That is, model pollutants carrying proton donor groups, such as phenylacetic acid, benzoic acid, benzamide, aniline and phenol, demonstrate an average binding energy that is 6 kcal mol^{-1} and 4

kcal mol^{-1} stronger than that of the water molecule at the adsorption site III and IV, respectively. On the other hand, model pollutants lacking a proton donor group, exhibit interaction energies that either similar to or weaker than the interactions between the water molecule and these adsorption sites. In PCM, interaction energies change for 1.6 kcal mol^{-1} in average, the overall trend remains unaltered.

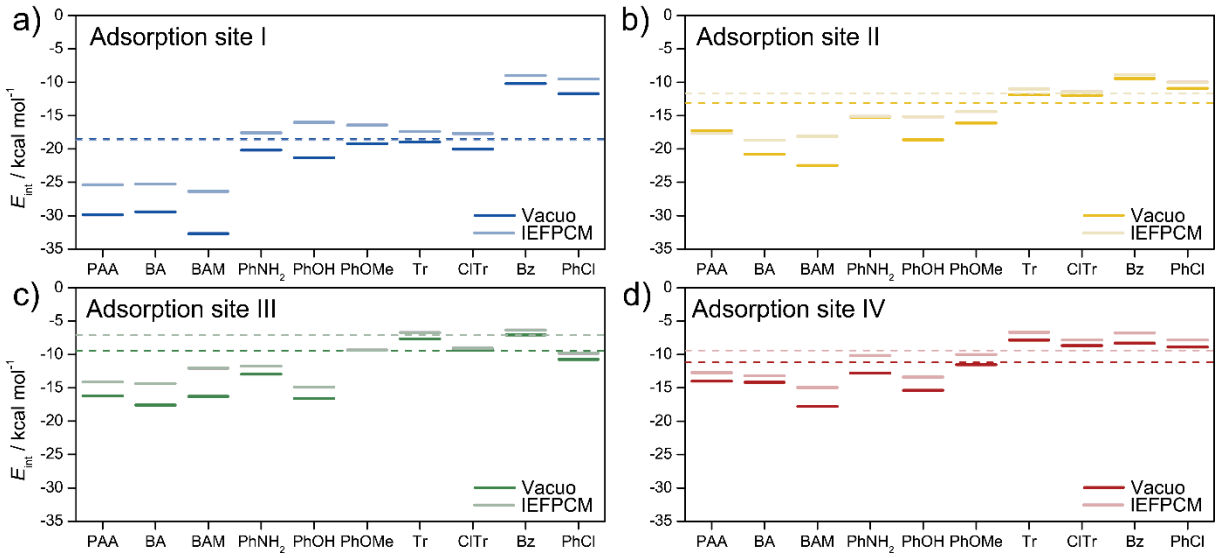

Figure 6. Interaction energies of the model pollutants and mPET on a) adsorption site I, b) adsorption site II, c) adsorption site III, and d) adsorption site IV calculated in vacuo and in implicit water as a solvent using IEFPCM model at M06-L level of theory and def2-SVP basis set. Dashed lines represent the interaction energies of water molecules.

IGMH analysis

The interaction energies of model pollutants and mPET did not show the same trend for all four adsorption sites. In general, the energies were consistent with the strength and number of hydrogen-bonds the model pollutants could form. Accordingly, the interaction energies of benzamide, phenylacetic acid and benzene depended the most on the adsorption site, while the interaction energies of benzene and chlorobenzene did not. To illustrate this, in **Figure 7** we show the scatter plots of weak interactions from IGMH analysis of benzamide and benzene interactions with the four adsorption sites of mPET. The scatter plot of benzamide interactions with the adsorption site I show the large contribution of hydrogen bonding. However, that contribution is reduced on the adsorption sites II, III, and IV. This is consistent with the numerical results as the difference between the interaction energies of benzamide with adsorption site I, where the interactions were strongest, and adsorption site III, where the interactions were weakest, was about 16 kcal mol^{-1}. In the case of benzene, however, the scatter plots are similar for all adsorption sites, because only the van der Waals interaction plays a role. This also suggests that π–π interactions, which could possibly form between the benzene ring of adsorption site II and the model pollutant, do not play an important role for the adsorption on mPET, as proposed by some experimental studies.[14,44] The scatter plots of weak interactions between all the model pollutants and water molecule, and all four adsorption sites can be seen in supporting materials in **Figure S7-S9**.

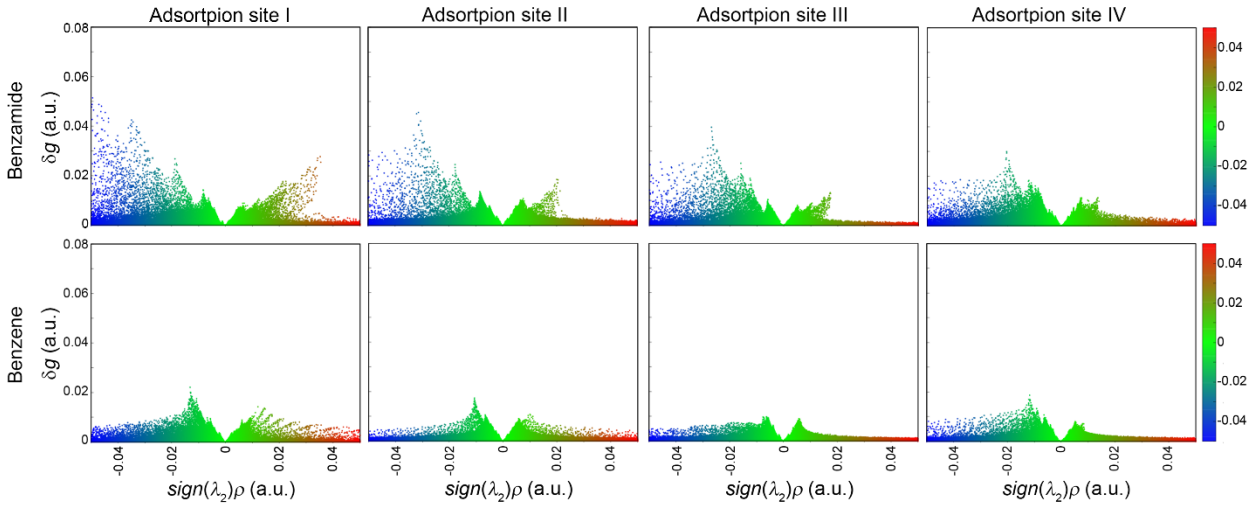

Figure 7. Scatter plots of IGMH analysis of weak interactions between benzamide and benzene, and all four adsorption sites of mPET. In the usual colouring scheme, the blue colour represents attractive interactions, the green colour represents van der Waals interactions, and the red colour represents non-bonding interactions.

10.1002/cphc.202300854

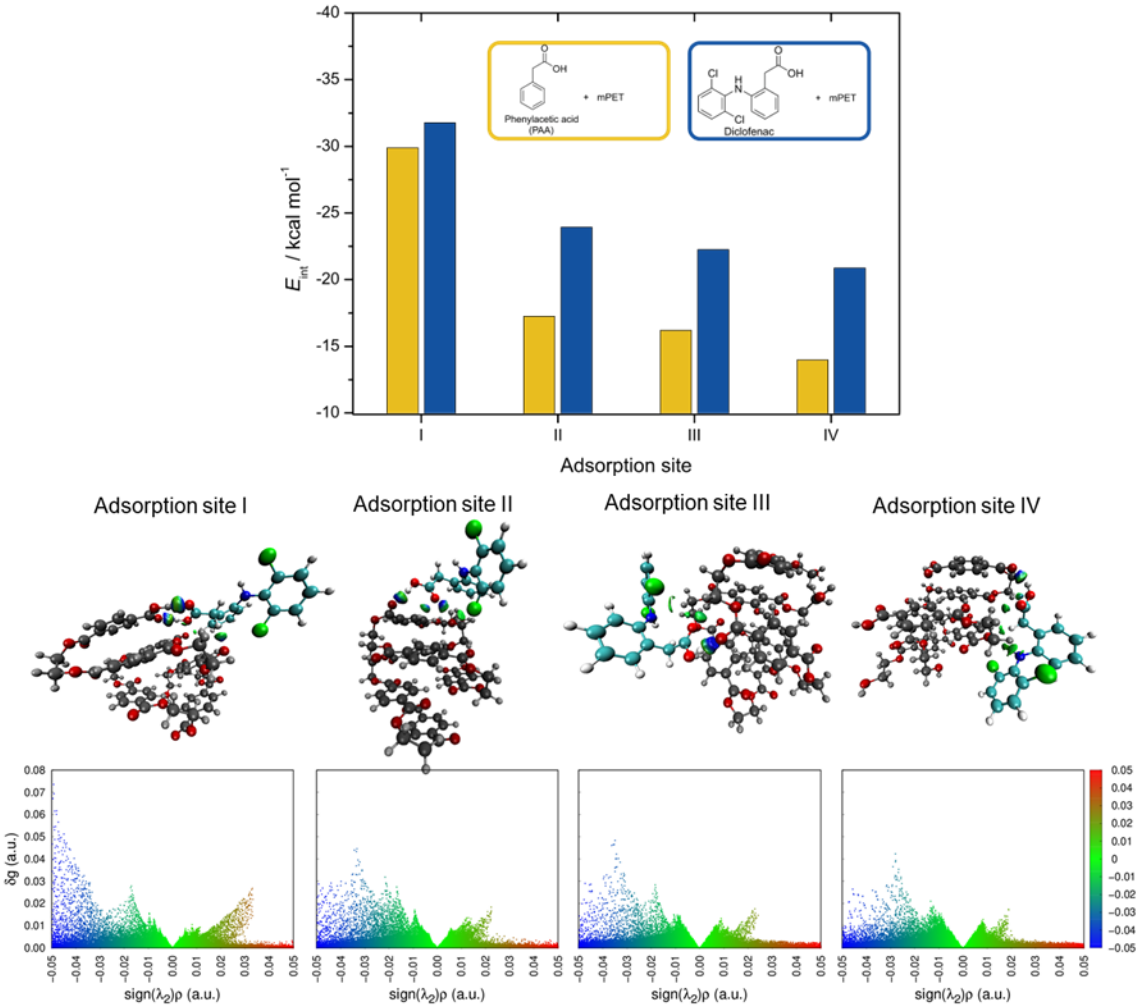

Figure 8. (top) Interaction energies of mPET and phenylacetic acid compared to interaction energies of mPET and diclofenac calculated by M06-L/def2-SVP method. Yellow/blue columns correspond to interaction energies between mPET and (phenylacetic acid)/(diclofenac). (bottom) Independent gradient model (IGMH) analysis scatter plots of weak interactions between diclofenac and mPET at all four adsorption sites. In the usual colouring scheme, the blue colour represents attractive interactions, the green colour represents van der Waals interactions, and the red colour represents non-bonding interactions.

To verify the qualitative validity of the above results based on selected fractions of the organic pollutants we studied the interaction of a common organic pollutant with mPET, namely, diclofenac and we compared the obtained results to those obtained for PAA. The results presented in **Figure 8** point out that for site I, the interaction energy for mPET with diclofenac is comparable to that of PAA. In contrast, at adsorption site II, the binding affinity of diclofenac with mPET markedly surpasses that of PAA, suggesting a notably stronger interaction at this particular site.

This pronounced affinity is consistently observed across sites III and IV. The IGMH analysis, shown in the same figure, further substantiates these findings by revealing a complex interplay of attractive forces, van der Waals interactions, and steric repulsions at these sites. Specifically, sites II, III, and IV demonstrate a convergence of multiple non-covalent interactions that are integral to the stabilization of the mPET-diclofenac complexes. The results of the IGMH analysis, paired with the interaction energy profiles, indicate that the strength of the binding should be linked to the structural attributes of the pollutants, namely, the size and flexibility of the molecules. Diclofenac, with its larger and more flexible molecular structure, appears to establish a more extensive network of interactions compared to its PAA fragment. This comprehensive network is likely facilitated by diclofenac's ability to adapt to the topography of the adsorption sites on mPET, forming multiple non-covalent bonds that reinforce the stability of the complex.

Finally, it is meaningful to demonstrate at this point the difference between folded mPET models and oligomeric chains. To do so, we compared the interaction energies of the model pollutants with terephthalic acid (TA) in two configurations represented in **Figure S1** which correspond to the adsorption sites I and II. All the details of those interactions are shown in **Figure S4** and **Figure S5** of the supporting materials. As seen in the results depicted in **Figure 9**, the difference between the interaction energies of the model pollutants with mPET and TA was negative for all model pollutants, suggesting that they bind strongly on the surface of mPET than on TA. This can be easily understood from the visual representations of the intermolecular interactions illustrated in **Figure 10.** As it is observed, the model pollutants can form multiple non-covalent interactions or hydrogen bonds with the neighbouring parts of mPET. This suggests that the adsorption mechanism of pollutants on micro and nano PET is different from the interaction with PET chains, which is consistent with other studies[19,20] and should be considered in future studies. The same trend is observed for the rest systems considered in this work (see **Figure S10-S14** of the supporting materials**)**.

10.1002/cphc.202300854

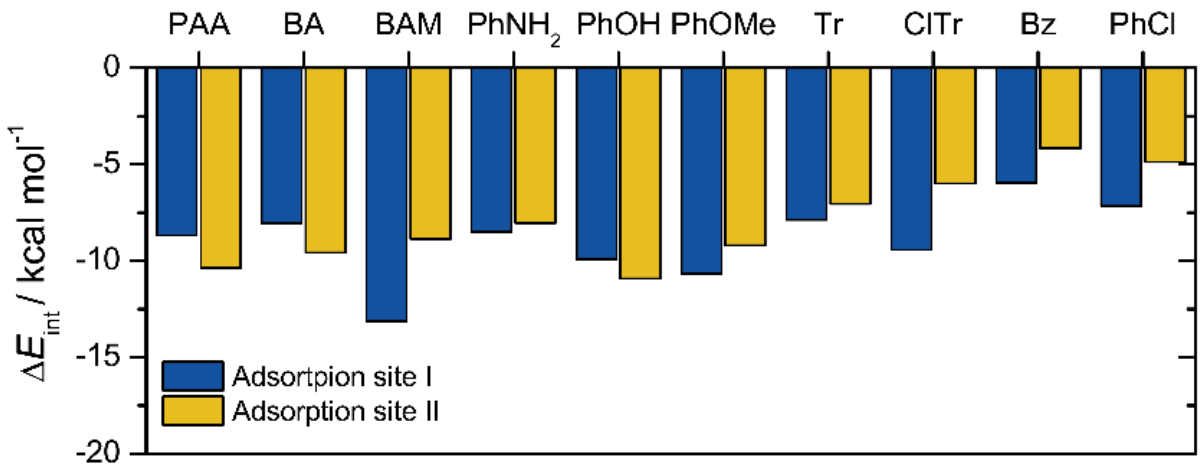

Figure 9. Difference between interaction energies of pollutants with mPET and terephthalic acid on adsorption sites I and II calculated by M06-L/def2-SVP method.

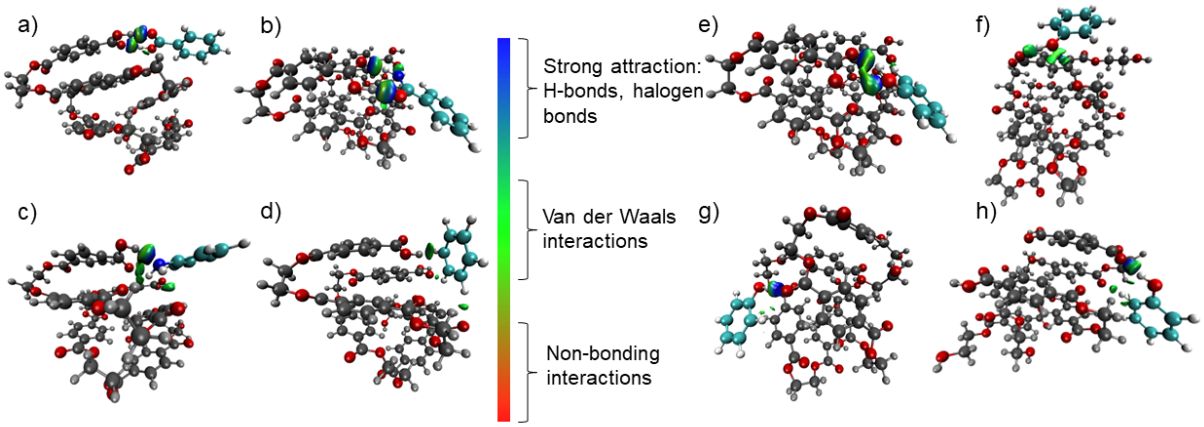

Figure 10. Schematic representations of the interactions between adsorption site I of mPET and a) benzoic acid; b) benzamide; c) aniline; d) benzene, and between phenol and mPET on e) adsorption site I; f) adsorption site II; g) adsorption site III; h) adsorption site IV analysed by independent gradient model (IGMH) and visualised on 0.01 a.u. isosurface. In the usual colouring scheme, the blue colour represents attractive interactions, the green colour represents van der Waals interactions, and the red colour represents non-bonding interactions.

Synergistic and ageing effects

To assess the significance of synergistic effects on the interaction of mPET with organic pollutants, we worked as follows. First, we optimized the structure of mPET with four phenols adsorbed on distant adsorption sites of mPET. Then, we gradually removed the phenols and re-optimized the structure at each step to obtain a series of optimized structures containing mPET and phenols. Finally, we calculated the interaction energies between each phenol and mPET without other phenols and with one, two, and three additional phenols adsorbed on the surface of mPET. The results are shown in **Figure 11**. Upon analyzing the obtained data, it becomes evident that the local interactions play a dominant role. Specifically, we see that the interaction energy for a particular phenol remains largely unchanged, even when additional phenols are introduced onto the mPET surface. This suggests that each phenol's interaction with mPET is primarily determined by its immediate surroundings on the mPET, rather than distant phenol molecules. From a quantum chemistry standpoint, this observation indicates that the forces acting at the individual adsorption sites, such as localized electron density shifts via polarization and specific orbital interactions, are crucial in dictating the interaction energy.

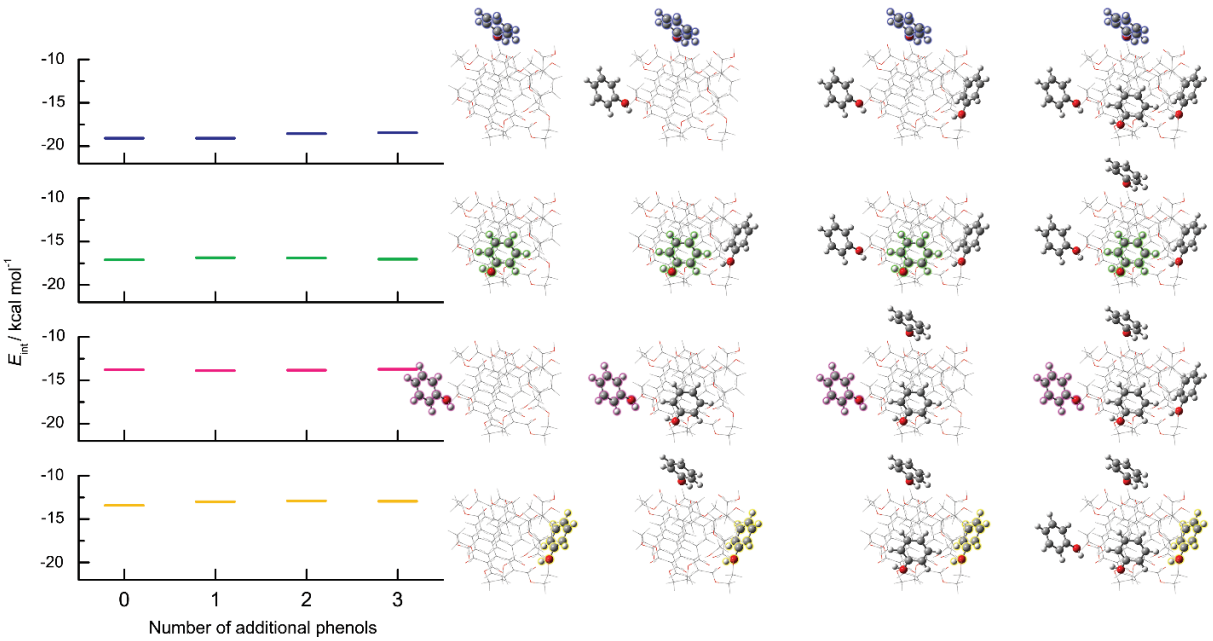

Figure 11. Interaction energies of phenol and mPET with no other phenols adsorbed and with multiple phenols adsorbed on different parts of mPET surface calculated at M06-L level of theory using def2-SVP basis set.. Highlighted phenol molecules correspond to ones whose interaction energies are calculated.

Microplastics in the environment are susceptible to photooxidative ageing. Ageing of MP can lead to morphological changes on the surface of MP and the formation of new oxygen containing functional groups such as hydroxyls, carboxyls, and ketones, which consequently can affect adsorption capacity. Experimental studies from the literature have shown that the aged PET MP generally has a higher adsorption capacity for organic pollutants than the pristine PET MP.[45]

Here, we present the aged PET as a modified pristine mPET with additional oxygen-containing groups on each monomer. The molecular structures of the modified monomers are shown in **Figure 12**. mPET–OH has two additional hydroxyl groups on each benzene ring of mPET. mPET–COOH has an additional carboxyl group on the carbon atom of the ethylene group, and mPET=O has an additional oxygen bonded through a double bond on this carbon atom.

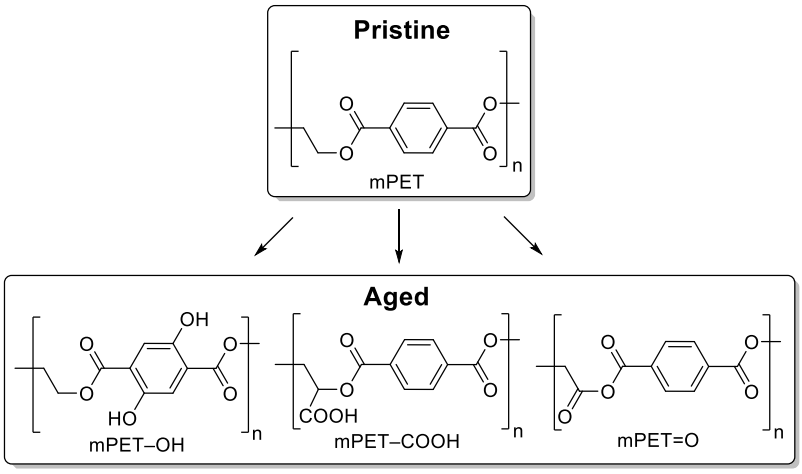

Figure 12. Molecular structure of pristine and aged model PET monomers.

To understand the effects of ageing on the adsorption interactions, we calculated the interaction energies of phenol with the pristine and aged mPETs at all four adsorption sites. The results are shown in **Figure 13**. Some minor variations in the interaction energies of phenol with pristine and aged mPETs are observed, which we attribute to the structural changes and repositioning of PET chains and phenol during the optimization process. However, there is no significant difference in the interaction energies. Therefore, we assume that the formation of oxygen-containing functional groups has no effect on the interactions between organic pollutants and PET MP. Ageing of PET MP could affect the adsorption capacity by providing more adsorption sites, since the aged particles generally have a larger specific surface area. Additionally, surface oxidation could lead to the formation of more adsorption sites able to form stronger

interactions with organic pollutants through hydrogen bonding. As seen from our model, adsorption site I that contains –COOH terminal group showed the strongest adsorption interactions with pollutants containing hydrogen bond donor and acceptor groups compared to other model adsorption sites.

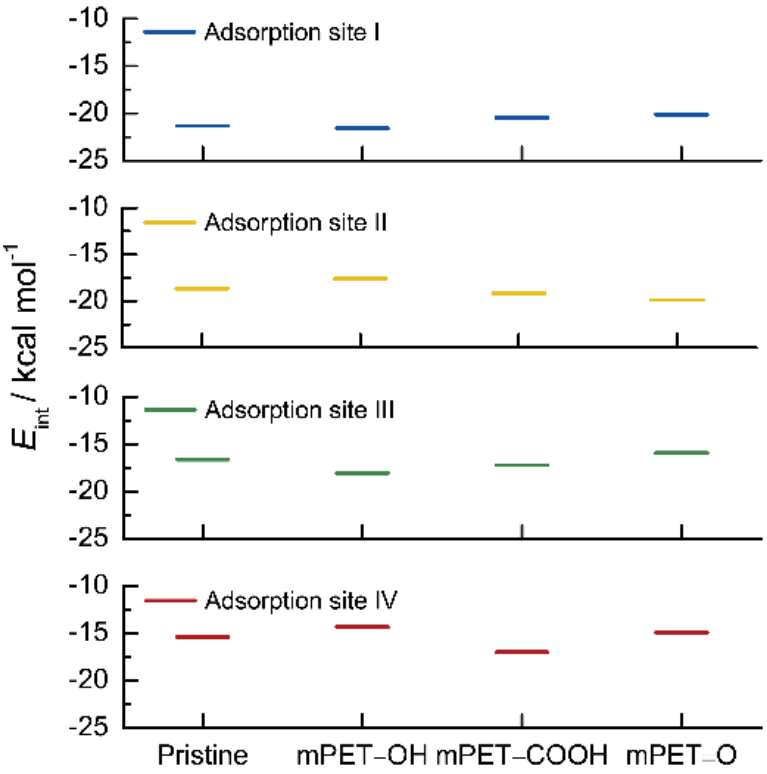

Figure 13. Interaction energies of phenol with pristine (mPET) and aged (mPET–OH, mPET–COOH, and mPET=O) PET models calculated at M06-L level of theory using def2-SVP basis set.

10.1002/cphc.202300854

Finally, we calculated the interaction energies of twelve phenols adsorbed on the surface of mPET–COOH. The structure is shown in **Figure 14**. The interaction energies of all twelve phenols ranged from –11.7 to –22.7 kcal mol^{-1}, with an average interaction energy of –17.2 kcal $mol.^{-1}$ This range of energies signifies a stable interaction across all twelve phenolic species with the mPET–COOH surface, suggesting that even small nanoparticles of aged mPET possess the capacity to adsorb a considerable number organic pollutants effectively.

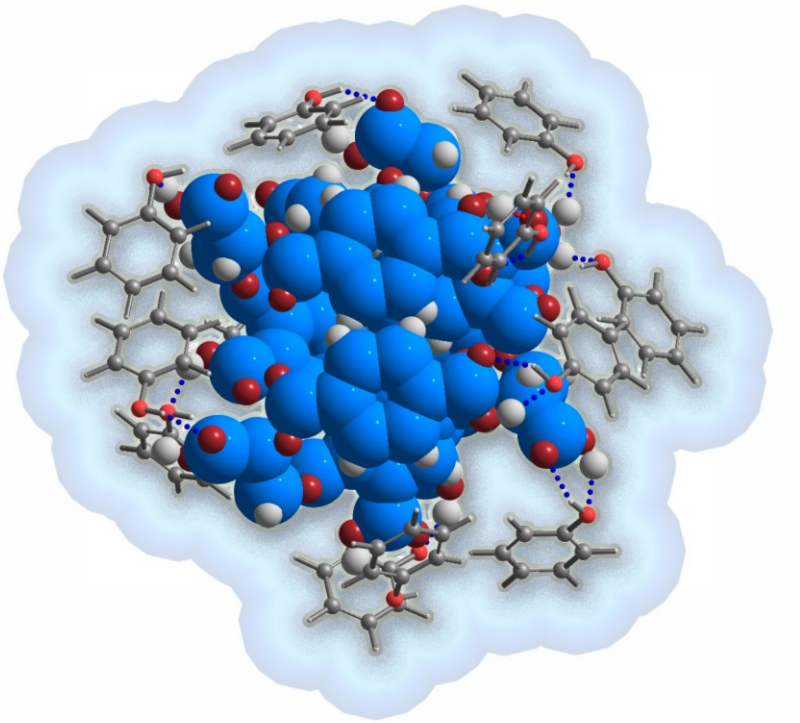

Figure 14. The structure of mPET-COOH with twelve phenols adsorbed optimized in gas phase at M06-L level of theory and def2-SVP basis set

Conclusion

In this work, we investigated the adsorption interactions of 10 small organic pollutants at different adsorption sites of the mPET surface. Our results show that the adsorption interactions between organic pollutants and mPET are weak, local interactions. The strongest interactions were between phenylacetic acid, benzoic acid, and benzamide and mPET at adsorption site I near the end of the chain containing the carboxyl group. The difference in the interaction energies of the pollutants was mainly related to the number of hydrogen bonds they could form with mPET. The

interactions of all the pollutants, except benzene and chlorobenzene, were dependent on the adsorption site. Benzene and chlorobenzene showed the weakest interaction energies with mPET at all adsorption sites. This is due to the fact that they cannot form hydrogen bonds and their interactions with mPET. The size of the mPET particles does not affect the interaction energies. Organic pollutants interact with the adjacent parts of the PET surface. For this reason, the interactions with a particle model PET were stronger than with the unfolded oligomeric chain model PET. The obtained results underscore the significance of understanding local molecular interactions when investigating adsorbate-adsorbent systems. Finally, from a computational point of view, our results suggest that particle model of MP should be used instead of unfolded oligomeric chains or other prototype models in the study and elucidation of interactions between organic pollutants and nano or micro-plastics.

Acknowledgements

We would like to acknowledge the financial support by the Croatian Science Foundation under the project *Microplastic in water; fate and behaviour and removal*, ***ReMiCRO*** (IP-2020-02-6033). A part of the research was performed using the computational resources provided by computer cluster Isabella based in SRCE – University of Zagreb, University Computing Centre. We also acknowledge the "Direction du Numérique" of the "Université de Pau et des Pays de l'Adour" for the computing facilities provided. Part of this work was granted access to the HPC resources of (CCRT/CINES/IDRIS) under the allocations 2022-AD010807031R1, 2023- AD010807031R2 made by GENCI (Grand Equipment National de Calcul Intensif).

References

[1] C. Wang, J. Zhao, B. Xing, *J. Hazard. Mater.* **2021**, *407*, 124357.

[2] D. Materić, H. A. Kjær, P. Vallelonga, J. L. Tison, T. Röckmann, R. Holzinger, *Environ. Res.* **2022**, *208*, 112741.

[3] M. Wagner, S. Lambert, in *Freshw. Microplastics Emerg. Environ. Contam.*, Springer International Publishing, Cham, **2018**, pp. 1–23.

[4] Y. Lu, Y. Zhang, Y. Deng, W. Jiang, Y. Zhao, J. Geng, L. Ding, H. Ren, *Environ. Sci. Technol.* **2016**, *50*, 4054–4060.

[5] L. Lei, S. Wu, S. Lu, M. Liu, Y. Song, Z. Fu, H. Shi, K. M. Raley-Susman, D. He, *Sci. Total Environ.* **2018**, *619–620*, 1–8.

[6] A. E. Rubin, I. Zucker, *Chemosphere* **2022**, *289*, DOI 10.1016/j.chemosphere.2021.133212.

[7] S. Liu, J. Wang, J. Zhu, J. Wang, H. Wang, X. Zhan, *Chemosphere* **2021**, *282*, 130967.

[8] X. Guo, J. Wang, *Mar. Pollut. Bull.* **2019**, *142*, 1–14.

[9] R. M. Razanajatovo, J. Ding, S. Zhang, H. Jiang, H. Zou, *Mar. Pollut. Bull.* **2018**, *136*, 516–523.

[10] B. Xu, F. Liu, P. C. Brookes, J. Xu, *Mar. Pollut. Bull.* **2018**, *131*, 191–196.

[11] X. Guo, C. Chen, J. Wang, *Chemosphere* **2019**, *228*, 300–308.

[12] Z. Liu, Q. Qin, Z. Hu, L. Yan, U. I. Ieong, Y. Xu, *Environ. Pollut.* **2020**, *265*, 114926.

[13] J. Li, K. Zhang, H. Zhang, *Environ. Pollut.* **2018**, *237*, 460–467.

[14] M. Munoz, D. Ortiz, J. Nieto-Sandoval, Z. M. de Pedro, J. A. Casas, *Chemosphere* **2021**, *283*, 131085.

[15] F. Liu, G. Liu, Z. Zhu, S. Wang, F. Zhao, *Chemosphere* **2019**, *214*, 688–694.

[16] M. Yang, D. Zhang, W. Chu, *SSRN Electron. J.* **2023**, *880*, 163261.

[17] Q. Mo, X. Yang, J. Wang, H. Xu, W. Li, Q. Fan, S. Gao, W. Yang, C. Gao, D. Liao, Y. Li, Y. Zhang, *Environ. Pollut.* **2021**, *291*, 118120.

[18] H. Yu, B. Yang, M. G. Waigi, F. Peng, Z. Li, X. Hu, *Chemosphere* **2020**, *261*, 127592.

[19] D. Cortés-Arriagada, *Environ. Pollut.* **2021**, *270*, 116192.

[20] D. E. Ortega, D. Cortés-Arriagada, *Environ. Pollut.* **2023**, *318*, 120860.

[21] D. Cortés-Arriagada, S. Miranda-Rojas, M. Belén, D. E. Ortega, V. B. Alarcón-Palacio, *Sci. Total Environ.* **2022**, *861*, 160632.

[22] D. Cortés-Arriagada, D. E. Ortega, *Sci. Total Environ.* **2023**, *891*, 164470.

[23] W. Liu, H. Tang, B. Yang, C. Li, Y. Chen, T. Huang, *Sci. Total Environ.* **2023**, *862*, 160786.

[24] H. A. Leslie, M. J. M. van Velzen, S. H. Brandsma, A. D. Vethaak, J. J. Garcia-Vallejo, M. H. Lamoree, *Environ. Int.* **2022**, *163*, 107199.

[25] L. C. Jenner, J. M. Rotchell, R. T. Bennett, M. Cowen, V. Tentzeris, L. R. Sadofsky, *Sci. Total Environ.* **2022**, *831*, 154907.

[26] Gaussian 16 revision C.01, M. J. Frisch, G. W. Trucks, H. B. Schlegel, G. E. Scuseria, M. A. Robb, J. R. Cheeseman, G. Scalmani, V. Barone, G. A. Petersson, H. Nakatsuji, X. Li, M. Caricato, A. V. Marenich, J. Bloino, B. G. Janesko, R. Gomperts, B. Mennucci, H. P. Hratchian, J. V. Ortiz, A. F. Izmaylov, J. L. Sonnenberg, Williams, F. Ding, F. Lipparini, F. Egidi, J. Goings, B. Peng, A. Petrone, T. Henderson, D. Ranasinghe, V. G. Zakrzewski, J. Gao, N. Rega, G. Zheng, W. Liang, M. Hada, M. Ehara, K. Toyota, R. Fukuda, J. Hasegawa, M. Ishida, T. Nakajima, Y. Honda, O. Kitao, H. Nakai, T. Vreven, K. Throssell, J. A. Montgomery Jr., J. E. Peralta, F. Ogliaro, M. J. Bearpark, J. J. Heyd, E. N. Brothers, K. N. Kudin, V. N. Staroverov, T. A. Keith, R. Kobayashi, J. Normand, K. Raghavachari, A. P. Rendell, J. C. Burant, S. S. Iyengar, J. Tomasi, M. Cossi, J. M. Millam, M. Klene, C. Adamo, R. Cammi, J. W. Ochterski, R. L. Martin, K. Morokuma, O. Farkas, J. B. Foresman, D. J. Fox, Gaussian Inc., Wallingford, CT, **2019**.

[27] P. J. Stephens, F. J. Devlin, C. F. Chabalowski, M. J. Frisch, *J. Phys. Chem.* **1994**, *98*, 11623–11627.

[28] C. Lee, W. Yang, R. G. Parr, *Phys. Rev. B. Condens. Matter* **1988**, *37*, 785–789.

[29] A. D. Becke, *J. Chem. Phys.* **1993**, *98*, 5648–5652.

[30] S. H. Vosko, L. Wilk, M. Nusair, *Can. J. Phys.* **1980**, *58*, 1200–1211.

[31] Y. Zhao, N. E. Schultz, D. G. Truhlar, *J. Chem. Phys.* **2005**, *123*, 161103.

[32] Y. Zhao, N. E. Schultz, D. G. Truhlar, *J. Chem. Theory Comput.* **2006**, *2*, 364–382.

[33] Y. Zhao, D. G. Truhlar, *Theor. Chem. Acc.* **2008**, *120*, 215–241.

[34] Y. Zhao, D. G. Truhlar, *J. Phys. Chem. A* **2006**, *110*, 5121–5129.

[35] S. F. Boys, F. Bernardi, *Mol. Phys.* **1970**, *19*, 553–566.

[36] S. Simon, M. Duran, J. J. Dannenberg, *J. Chem. Phys.* **1996**, *105*, 11024–11031.

[37] J. Tomasi, B. Mennucci, R. Cammi, *Chem. Rev.* **2005**, *105*, 2999–3093.

[38] C. Lefebvre, J. Klein, H. Khartabil, J. C. Boisson, E. Hénon, *J. Comput. Chem.* **2023**, *44*,

1750–1766.

[39] C. Lefebvre, H. Khartabil, J.-C. Boisson, J. Contreras-García, J.-P. Piquemal, E. Hénon, *Chemphyschem* **2018**, *19*, 724–735.

[40] T. Lu, Q. Chen, *J. Comput. Chem.* **2022**, *43*, 539–555.

[41] W. Humphrey, A. Dalke, K. Schulten, *J. Mol. Graph.* **1996**, *14*, 33-38.

[42] T. Williams, C. Kelley, many others, **2023**.

[43] T. Lu, Q. Chen, *J. Phys. Chem. A* **2023**, *127*, 7023–7035.

[44] J. Lin, D. Yan, J. Fu, Y. Chen, H. Ou, *Water Res.* **2020**, *186*, 116360.

[45] F. Kong, X. Xu, Y. Xue, Y. Gao, L. Zhang, L. Wang, S. Jiang, Q. Zhang, *Arch. Environ. Contam. Toxicol.* **2021**, *81*, 155–165.